Nuclear Inst. and Methods in Physics Research, A 985 (2021) 164669

Contents lists available at ScienceDirect

Nuclear Inst. and Methods in Physics Research, A

journal homepage: www.elsevier.com/locate/nima

Initial development and testing of dysprosium-based scintillators for digital transfer method neutron imaging

Aaron E. Craft [a,*], William C. Chuirazzi [a,b], Christian Grünzweig [c], Manuel Morgano [c], Eberhard H. Lehmann [c]

[a] Idaho National Laboratory, PO Box 1625, MS 6000, Idaho Falls, ID 83415, USA
[b] Nuclear Engineering Program, Department of Mechanical and Aerospace Engineering, The Ohio State University, Columbus, OH 43210, USA
[c] Paul Scherrer Institute, Laboratory for Neutron Scattering and Imaging, CH-5232 Villigen PSI, Switzerland

ARTICLE INFO

Keywords:
Neutron imaging
Scintillator screen
Indirect transfer method
Digital imaging

ABSTRACT

A new type of scintillator screen consisting of a ZnS scintillator with a dysprosium neutron converter is explored in a joint effort between Idaho National Laboratory (INL) and Paul Scherrer Institute (PSI). In contrast with a traditional prompt ^{6}Li or Gd converters, a dysprosium converter generates a latent image as neutron activated dysprosium produces an isotope which decays with half-lives of 1.26 min and 2.3 h and the decay radiation excites the ZnS scintillator. The activated scintillator screen is physically transported out of the neutron beam and away from radioactive samples into the imaging apparatus and emits photons as the screen decays, which are read by a digital camera. This technology bridges the gap between traditional indirect transfer radiography and modern digital camera-based systems. This paper describes initial development of dysprosium-based scintillator screens and the results of initial tests performed at PSI. Some screen variants exhibit sufficient light output to produce good quality radiographs in a matter of minutes. The basic spatial resolution measured using a Siemens star is approximately 300 μm. This work demonstrates for the first time that indirect digital transfer method neutron imaging is a plausible method of imaging highly radioactive sources such as irradiated nuclear fuel.

1. Introduction

Neutron radiography yields the most extensive data of any non-destructive technique currently available for assessing the internal condition of irradiated nuclear fuel [1]. Traditionally, irradiated materials with high levels of gamma radiation have been imaged by transfer method neutron radiography using film or image plates [2–6]. With the transfer method, a cassette containing converter foils is positioned behind an object in the neutron beam. Neutrons passing through the object activate the converter foils, creating a latent image in the pattern of activation corresponding to the neutrons passing through the object. The cassette is then removed from the beam and the activated converter foils are placed in contact with an imaging sensor, such as film [2], an image plate [3–5], or even mixed-dysprosium image plates [6]. The decay radiation exposes the sensor, which is then processed to produce a radiographic image. While the transfer method of neutron radiography is both labor intensive and time consuming, it is entirely insensitive to gamma rays, making it ideal for imaging highly radioactive samples.

Advantages of modern digital neutron radiography systems include quicker acquisition times, higher detection efficiency, position stability, high spatial resolution, and flexibility of field-of view. In digital camera-based neutron radiography, a digital camera is placed in a light tight box outside the neutron beam and optically coupled using a mirror to a neutron-sensitive scintillator located in the neutron beam. The object is placed in the neutron beam in front of the scintillator screen for examination. The scintillator materials are sensitive to gamma rays in the beam and emitted from radioactive samples, which fogs the image and degrades signal-to-noise ratio of the resulting image.

Traditional scintillator screens for digital neutron radiography use promptly-decaying neutron converters such as ^{6}Li or gadolinium. This work examines screens composed of scintillator material with activated neutron converters that exhibit a long half-life, such as neutron activated dysprosium isotopes, with main decay times of 1.3 min and 2.3 h. For such screens, a dysprosium converter generates a latent image as activated dysprosium decays and the decay radiation excites the scintillator. This novel approach integrates the gamma insensitivity of the transfer method with digital neutron radiography's benefits of quicker imaging times, ease of use, and higher detection efficiency.

This study builds upon previous work of designing a scintillator screen that replaces the prompt-decaying converter with a slower-decaying dysprosium foil [7]. The work reported in this paper improves

* Corresponding author.
E-mail addresses: aaron.craft@inl.gov (A.E. Craft), william.chuirazzi@inl.gov (W.C. Chuirazzi), christian.gruenzweig@psi.ch (C. Grünzweig), manuel.morgano@psi.ch (M. Morgano), eberhard.lehmann@psi.ch (E.H. Lehmann).

https://doi.org/10.1016/j.nima.2020.164669
Received 9 March 2020; Received in revised form 15 June 2020; Accepted 16 September 2020
Available online 19 September 2020

upon previous work on various combinations of scintillator materials and dysprosium converters with a more in-depth analysis of loading and decay times, effective spatial resolution, and integrated light output.

2. Dysprosium-based scintillator screens

Natural dysprosium includes seven stable isotopes, but ^{164}Dy (natural abundance of 28.18%) is the isotope of interest for neutron imaging purposes. Neutron activation of ^{164}Dy creates radioactive nuclei with two decay paths, described in Eqs. (1) and (2). The longer decay path with a half-life of 2.33 h is used for transfer method neutron radiography where radiographs are produced after several hours of decay [2]. The quicker decay path is ideal for digital transfer method neutron radiography because its shorter half-life of 1.26 min allows it to create neutron radiographs in a matter of minutes. Producing radiographs quickly is particularly useful for neutron tomography, where many radiographs must be acquired to generate a full set of images suitable for tomographic reconstruction [8]. However, the longer lived 2.33-hour half-life can cause the dysprosium-based scintillator screens to retain an image history that more severely impacts the neutron image with increased exposure to the neutron beam. Digital transfer method neutron radiography requires either shorter exposure times (~10-20 min) or additional image processing to address the influence of the 2.33-hour half-life.

$$^{164}_{66}Dy + n \xrightarrow{\sigma_a \approx 1700b} {}^{165}_{66}Dy \xrightarrow{t_{1/2}=2.33h} \beta^- + {}^{165}_{67}Ho \quad (1)$$

$$^{164}_{66}Dy + n \xrightarrow{\sigma_a \approx 1000b} {}^{165m}_{66}Dy \xrightarrow{t_{1/2}=1.26m} IT_\gamma + {}^{165}_{66}Dy \quad (2)$$

A range of scintillator screens were fabricated for parametric study, each using ZnS:Cu as a phosphor. The range of screens represents various phosphor grain sizes, absorber material form (i.e. metallic dysprosium foil or Dy_2O_3), substrate, scintillator to converter mixture ratio, and phosphor thickness. Three ZnS:Cu grain sizes were employed: fine (d_{50} = 3.05 μm), medium (d_{50} = 4.67 μm) and large (d_{50} = 9.67 μm). Some screens had the ZnS:Cu mixed directly with Dy_2O_3 on an aluminum substrate while others had ZnS:Cu deposited on a dysprosium foil. A total of 23 screens were fabricated, each with an area of 25 mm × 25 mm. Table 1 lists the 23 scintillator screens and their characteristics. The logic and intent behind the parameter choices for each screen are as follows:

- Screens #1-#4, containing large phosphor grains, an aluminum substrate, and an absorber to phosphor ratio of 1:2 by weight, were manufactured to mimic conventional neutron imaging scintillators screens. Varying screen thicknesses explore the effect of thickness on image resolution and light output.
- Screens #5 and #6 are similar to screen #3, only different in absorber-to-phosphor ratio, in case the standard 1:2 mixture which is optimal in the case of ^{6}LiF-ZnS based scintillator is not ideal with dysprosium.
- In screen #7, the absorber is applied differently than all the other screens. While for all the other screen the absorber is mixed in the matrix, in this case the Dy-containing molecule is applied by spray-drying.
- Screens #8-#10 vary the phosphor grain size to explore its effects on image quality.
- Screens 11–14 are the same as screens 1–4 but substitute the aluminum substrate for a 125 μm thick dysprosium foil. While this provides additional neutron absorbing material, it may also cause self-shielding that would reduce the neutron intensity in the coating.
- Screens #15 and #16 are the same as screens #5 and #6, with a dysprosium foil (125 μm thick) substrate.
- Screens #17 to #19 are the same as screens #8-#10, with a dysprosium foil (125 μm thick) substrate.

Table 1
Parameters for the set of 23 scintillator screen samples.

Screen number	Substrate	Absorber material	Phosphor (grain size)	Wt. ratio (Dy_2O_3:ZnS)	Thickness [um]
1	Al-plate	Dy_2O_3	ZnS:Cu (large)	1:2	30
2	Al-plate	Dy_2O_3	ZnS:Cu (large)	1:2	50
3	Al-plate	Dy_2O_3	ZnS:Cu (large)	1:2	100
4	Al-plate	Dy_2O_3	ZnS:Cu (large)	1:2	200
5	Al-plate	Dy_2O_3	ZnS:Cu (large)	1:1	75
6	Al-plate	Dy_2O_3	ZnS:Cu (large)	1:3	100
7	Al-plate	$Dy(O_2CH)_3$	ZnS:Cu (medium)	1:2	60
8	Al-plate	Dy_2O_3	ZnS:Cu (large)	1:2	90
9	Al-plate	Dy_2O_3	ZnS:Cu (medium)	1:2	100
10	Al-plate	Dy_2O_3	ZnS:Cu (fine)	1:2	100
11	Dy-Foil	Dy_2O_3	ZnS:Cu (large)	1:2	35
12	Dy-Foil	Dy_2O_3	ZnS:Cu (large)	1:2	50
13	Dy-Foil	Dy_2O_3	ZnS:Cu (large)	1:2	100
14	Dy-Foil	Dy_2O_3	ZnS:Cu (large)	1:2	225
15	Dy-Foil	Dy_2O_3	ZnS:Cu (large)	1:1	85
16	Dy-Foil	Dy_2O_3	ZnS:Cu (large)	1:3	100
17	Dy-Foil	Dy_2O_3	ZnS:Cu (large)	1:2	100
18	Dy-Foil	Dy_2O_3	ZnS:Cu (medium)	1:2	100
19	Dy-Foil	Dy_2O_3	ZnS:Cu (fine)	1:2	100
20	Dy-Foil	none	ZnS:Cu (large)	pure	60
21	Dy-Foil	none	ZnS:Cu (large)	pure	100
22	Dy-Foil	none	ZnS:Cu (large)	pure	200
23	Dy-Foil	none	ZnS:Cu (fine)	pure	100

- Screens #20 to #22 are the same as screens #11-#13, with a dysprosium foil (125 μm thick) as substrate, but no absorber dispersed in the matrix. This is to potentially isolate the effect of the dispersion of the absorber as compared to absorption only in a dysprosium substrate.
- Screen 23 is the same as screen #19 (fine ZnS:Cu grains) without the absorber dispersed in the matrix.

3. Experiment setup and data processing

Scintillator screens were tested in PSI's Neutron Transmission Radiography (NEUTRA) thermal beamline at the second measurement position. This position places the samples 9.876 m away from the target center and 7.292 m from the aperture. The neutron flux is 9.8×10^6 n/cm^2/s/mA at the image plane with an L/D ratio of 350 and is proportional to the proton current (~1.5 mA) irradiating the SINQ target. [9]. During measurements, the Ultra Cold Neutron Source at SINQ was non-operational, ensuring a stable beam and therefore minimizing fluctuations in the neutron flux and energy spectrum.

The scintillators were placed in a 3 × 3 array on an aluminum substrate in the neutron beamline. An Andor Neo sCMOS camera, containing a pixel array of 2160 × 2560 with 16-bit dynamic range, housed in PSI's midi-box design captured neutron radiographs [10]. The camera was water-cooled to maintain a temperature at −25 °C. Radiographs were acquired during exposure to the neutron beam (referred to as "loading"), then the beam was turned off and additional images were acquired while the screens decayed without neutron exposure (referred to as "decay"). The screens were exposed to the beam for 1, 5 and 10 min with the camera taking a total of 30, 150 and 300 radiographs, respectively, each with an integration time of 2 s. After the exposure, the beam was turned off and the additional sets of radiographs were acquired as the activated screens decayed. A total of 150 decay images, each integrated for a total of 2 s, were recorded by the camera for a total of 5 min decay time for all tests. Upon completion of a set of measurements, the array of screens was removed from the beamline and replaced with another 3 x 3 array. Fig. 1 shows an example image demonstrating location of the 3×3 array of screens in the image field of view.

After testing all 23 screens, the seven screens that produced the highest light output were subjected to further testing. These screens

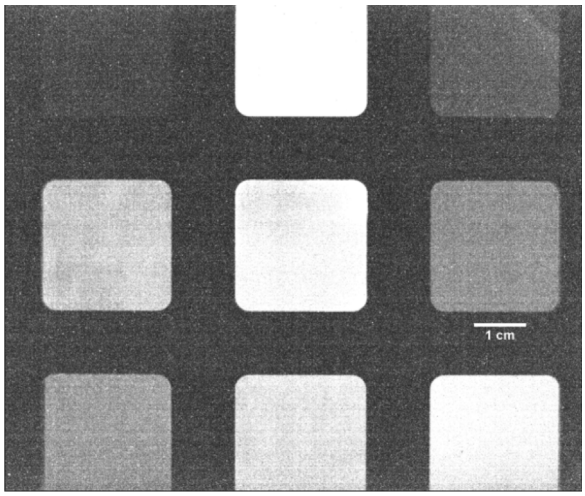

Fig. 1. Integrated neutron radiographs of screens 1–9 taken with 10 min of beam exposure and 5 min of decay.

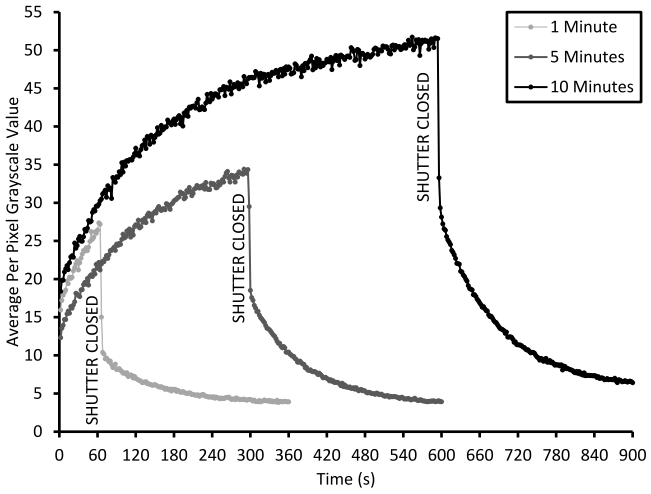

Fig. 2. The light output of a representative scintillator screen (#4) over time. The same scintillator screen was sequentially exposed to the beam for 5-min, 1-min, then 10-min loading times. After each exposure, the neutron shutter was closed and the light output during the decay phase was measured for 5 min.

underwent loading cycles of 5, 10 and 20 min with a decay time of 10 min. Spatial resolution was also measured for these screens.

A flat-field correction was taken with a standard ^{6}LiF/ZnS scintillator to account for the beam nonuniformity. Ten flat-field and ten dark-field images were acquired. A 2×2-pixel median filter was applied to remove outliers such as gamma-ray spots, then the ten images were averaged together to form one flat-field image and one dark-field image. The average dark-field image was subtracted from the open beam image, then the flat-field image was divided by its maximum to normalize the image to 1. Each image taken with the dysprosium-based screens were multiplied by the normalized flat-field image to correct for beam nonuniformity.

4. Results and discussion

4.1. Light output

Light output was measured by taking the average per pixel grayscale level over an area as large as possible over the scintillator. Measuring the average grayscale value in each neutron radiograph produced a plot of grayscale value over time. These measurements were taken for each of the 23 scintillator screens. As an example, Fig. 2 shows the light outputs of Screen #4 for 1-min, 5-min, and 10-min loading times and 5-min decay times. Measurements were taken sequentially: first the 5-min exposure, then the 1-min exposure, and then the 10-min exposure. There is a build-up of residual activity that is visible at $t = 0$ in Fig. 2 due to the 2.33 h half-life of ^{165}Dy.

Light output from the decay phase must be large enough to allow the imaging camera to capture a useful signal above the camera noise from individual pixels. Decay light output was measured by integrating the total counts per pixel each scintillator released once it was no longer under neutron exposure. The integrated light output from the decay phase should represent high enough gray value to produce a useful digital neutron image (e.g. greater than 1000 gray values). The results of integrating the decay light output are shown in Fig. 3. Screens #4, #14 and #22 demonstrated the highest decay light output, and light output increased for longer exposure times up to 10 min. In general, screens with thicker phosphor layers exhibited higher light output.

The loading and decay times of each scintillator are important parameters for designing an imaging system using the digital transfer method. While there are many reactions that take place in dysprosium in a neutron field, the average decay half-life is expected to be around the 1.26-min half-life of ^{164}Dy because this will be the dominant reaction exhibited in the first ten minutes of decay. The loading and decay curves in Fig. 2 were separately fitted using Eq. (3) for the loading curve and Eq. (4) for the decay curve. Curve fitting produced calculated loading constants (δ) and decay constants (λ) for each of the 23 screens using the following equations. Doubling time is calculated as $\ln 2/\delta$ and half-life is calculated as $\ln 2/\lambda$.

$$Loading:\ I(t) = I_{offset} - I_{saturation}\left(e^{-\delta_1 t} + e^{-\delta_2 t}\right) \quad (3)$$

$$Decay:\ I(t) = I_{offset} + I_{saturation}\left(e^{-\lambda_1 t} + e^{-\lambda_2 t}\right) \quad (4)$$

where $I(t)$ is the grayscale value as a function of time, I_{offset} is the gray value at the beginning of the loading phase and the end of the decay phases, $I_{saturation}$ is the gray value as $t \to \infty$, t is the time, λ_1 is the decay constant of the shorter-lived isotope, λ_2 is the decay constant of the dysprosium isotope with the 2.33-hour half-life, δ_1 is the loading constant of the shorter-lived isotope, and δ_2 is the loading constant of the dysprosium isotope with the 2.33-hour half-life. The doubling times and half-lives were calculated keeping λ_2 and δ_2 constant based on the 2.33 half-life decay path, then fitting the equations to solve for λ_1 and δ_1.

Fig. 4 shows an example, Screen #4, of the curve-fitting of a loading curve and a decay curve. The parameters λ and δ, extracted from the curve fits, are used to calculate the doubling time and half-life, respectively.

The resulting doubling times and half-lives are shown in Figs. 5 and 6. Screens #11-#18, fabricated with both a dysprosium substrate and Dy_2O_3 mixed with the phosphor, have the longest doubling times. Screens #1-#10, which have Dy_2O_3 mixed with the phosphor on an aluminum substrate, exhibited the shortest doubling times. Screens #19-#23, fabricated with phosphor on a dysprosium substrate, displayed doubling times shorter than screens #11-#18 but longer than screens #1-#10.

The decay times are relatively constant (see Fig. 6), with an exception of Screen #7 which employed spray-drying to incorporate dysprosium into the screen. However, the half-lives which are approximately 1 min instead of ^{164}Dy's 1.26-min half-life, are about 70% of the expected value. Dysprosium has seven stable isotopes. One possible cause for the shorter-than-expected half-life is potential impurities, but the reported impurities of the dysprosium used in this study are negligible and do not have short half-lives. The shorter-than-expected half-life is more likely caused by short-lived metastable isomers that decay into stable isotopes.

Based on the integrated decay light outputs shown in Fig. 3, screens #3, #4, #13, #14, #20, #21 and #22 were selected for further testing

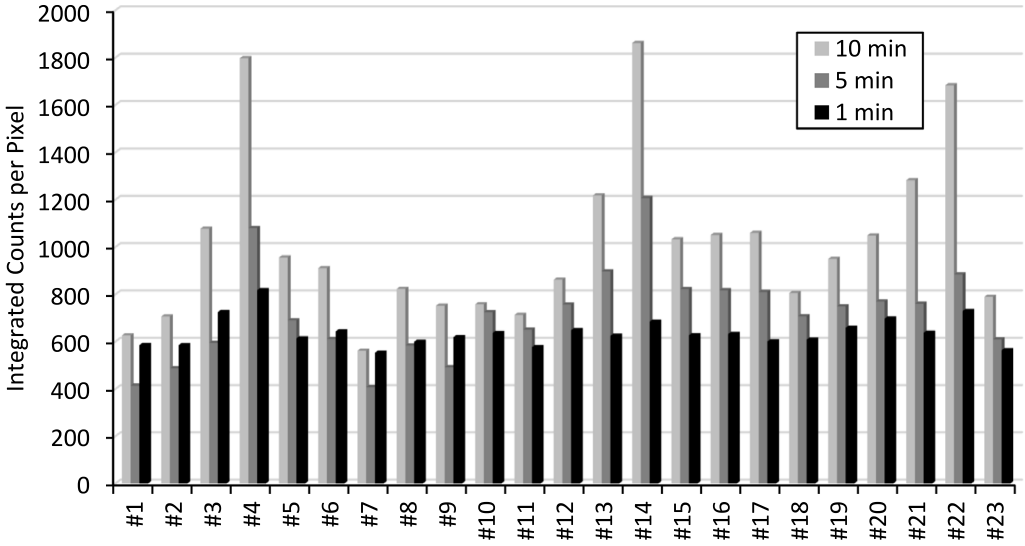

Fig. 3. Experimentally measured integrated light output during the decay phase. Scintillators are exposed to the beam for 1, 5 and 10 min followed by 5 min of decay time.

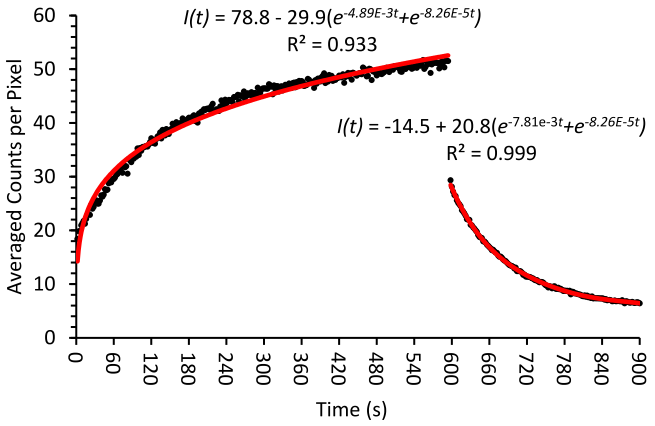

Fig. 4. Curve fits for both loading and decay phases of screen #4. Black data points represent the experimental data and the solid red line represents the fitted curve.

due to their high light output compared to the rest of the screens. These seven screens were subjugated to an extended exposure in the beamline with loading times of 5, 10 and 20 min followed by a 10-min decay time. The purpose of these experiments was to observe if the doubling time and half-life measurements stabilized with longer loading times.

Fig. 7 shows the resulting doubling times for the seven screens. The doubling time increases with loading time because the longer-lived isomer with a half-life of 2.33 h becomes more prominent with increased loading times. This data suggests that longer doubling times are associated with an increased amount of dysprosium in the scintillator screen.

Doubling time increases with longer exposure times up to 20 min, so secular equilibrium during the loading phase has not been reached. This is because the 2.33-hour half-life isomer takes 15.5 h to achieve 99% saturation. However, the 1.26-min half-life isomer achieves 99% saturation in just 8.4 min. The short-lived isomer is the reaction of interest for transfer method digital neutron radiography because it should result in shorter acquisition times than the longer-lived isomer.

Figs. 7 and 8 show the doubling-times and half-lives of the seven top performing screens under longer loading and decay times. Longer exposure time introduces the possibility of building up activity from the longer-lived ^{165}Dy isotope with a 2.33-hour half-life. Measurements with the 20-min loading time were taken first, then the 10-min loading time, followed by the 5-min loading time. The results vary slightly compared to the previous measurements which is most likely caused by the longer irradiation times building up longer-lived activity from ^{165}Dy, which has a half-life of 2.33 h. Similar to the behavior exhibited in previous doubling time measurements shown in Fig. 5, Fig. 7 also shows that saturation has still not been reached after 20 min loading time. Fig. 8 shows that the half-life measurements were similar to previous results shown in Fig. 6, confirming that the observed half-lives were about 1 min.

Fig. 9 shows the integrated grayscale counts per pixel during the decay phase. These grayscale values are all >1500, which is not near 80% of saturation desired for the 16-bit depth (max grayscale value is 65535) for high-end digital cameras, but is sufficient for imaging purposes. Screen #14 exhibits the highest light output in both series of tests. Although their relative light output varied with exposure times, screens #4 and #22 are shown to be the next brightest. These three screens are the thickest, therefore they have the greatest neutron detection efficiency. More neutron interactions will ultimately produce more photons in the phosphor, resulting in a greater light output. These results suggest that having dysprosium both in a thick foil and in the absorber-matrix produces the highest light output due to increased probability of neutron-absorber interactions.

Comparing screens 4 and 22, they produce roughly the same light output. They have the same thickness of phosphor, but #4 has the dysprosium converter mixed with the phosphor and #22 has phosphor on a dysprosium foil. However, screen #14 has dysprosium converter both mixed with the phosphor and as a substrate, but the light output is less than the sum of screens #4 and #22. This is because, for screen #22, the neutron flux must first penetrate the dysprosium substrate before interacting with the layer of mixed converter and phosphor. The mixed converter and phosphor layer of screen #22 would, therefore, experience lower neutron flux compared to that of screen #4.

4.2. Spatial resolution

Spatial resolution was measured for the seven screens that exhibited the highest light output. A Siemens star test pattern was attached to each screen and twenty frames were acquired, ten in the direct beam and ten with the beam closed, with 1-min for each frame. Each image underwent post-processing as previously described and the frames were averaged together to get the image shown in Fig. 10. Resolution was taken with a tangential line profile along the circle's circumference, starting at the center of the Siemen's star and extending until the line-pairs become visible.

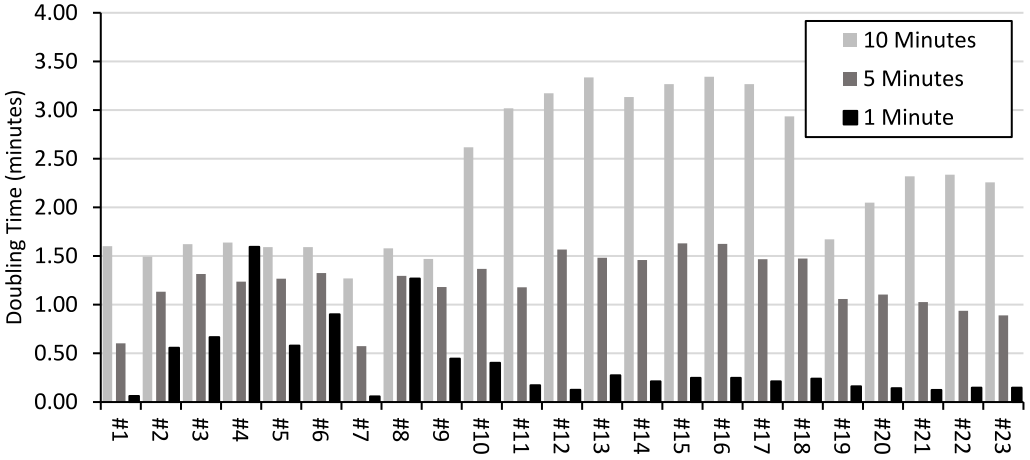

Fig. 5. Doubling times derived from curve fitting for all 23 scintillator screens with 1-, 5- and 10-min loading times.

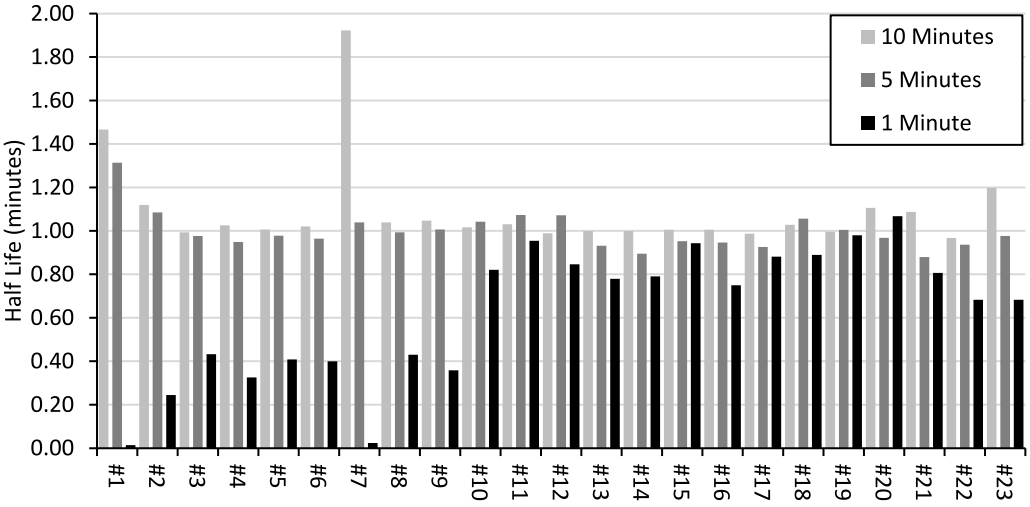

Fig. 6. Half-lives derived from curve fitting for all 23 scintillator screens with 1-, 5- and 10-min loading times.

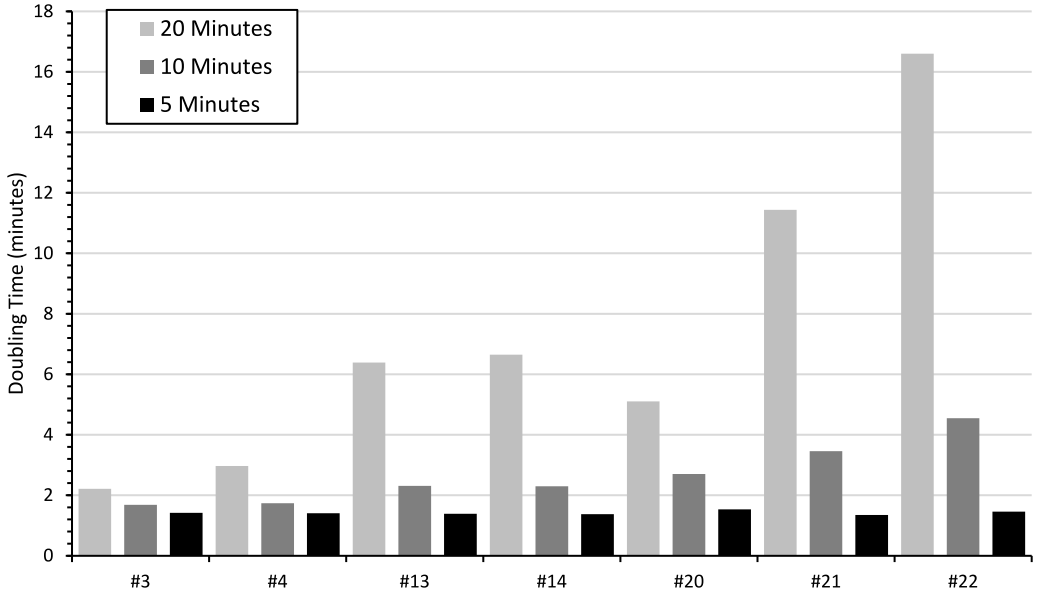

Fig. 7. Doubling times of the seven screens producing the highest light output under 20, 10 and 5 min of loading time.

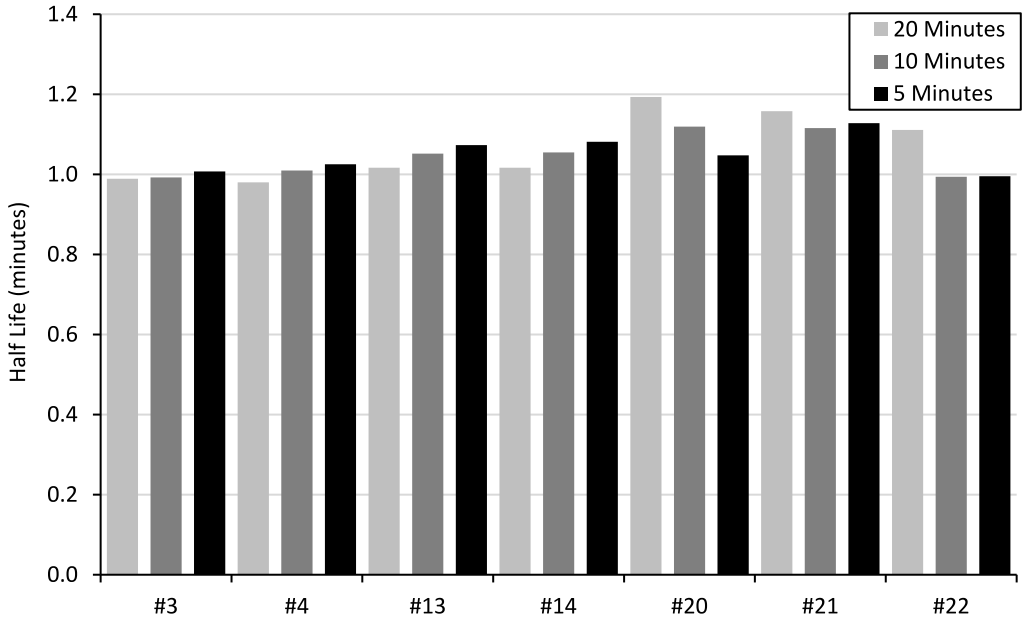

Fig. 8. Half-lives of the screens after observing 10 min of decay time.

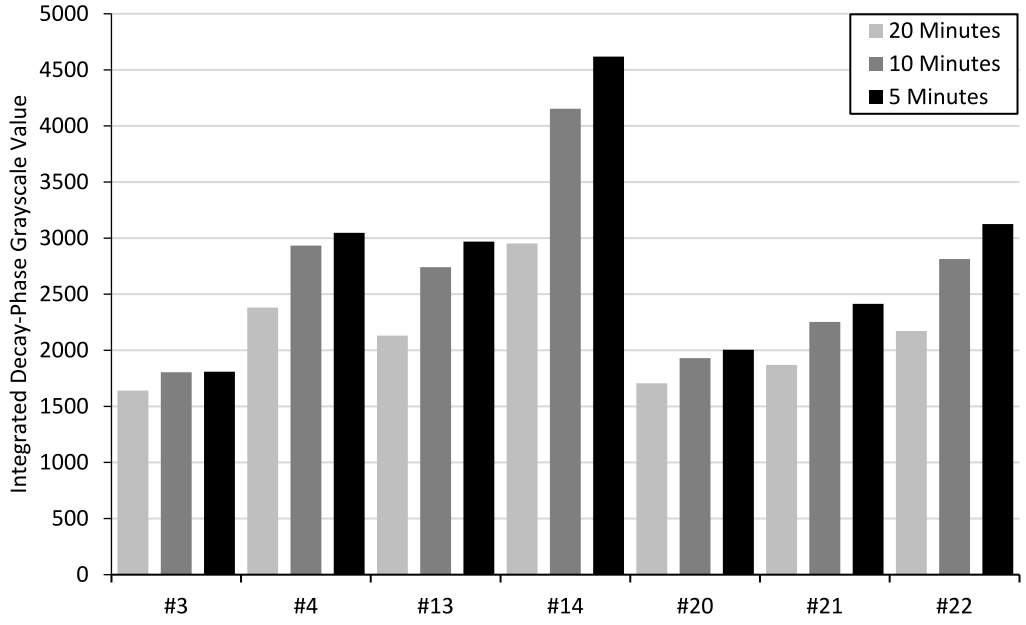

Fig. 9. Total counts of each scintillator screen during decay. Subsequent exposures have higher counts, even though irradiation time was lower, due to an increased activation from previous measurements.

The dysprosium screens exhibit an effective spatial resolution of approximately 300 μm which is 50% lower than the 200 μm resolution measured with a standard ^{6}LiF/ZnS with a 200 μm thickness. The beta particle emitted from the ^{165}Dy and the isomeric transition photon from ^{165m}Dy deposit energy across a longer range from the initial absorption site compared to the daughter products of ^{6}Li(n, α)^{3}H reaction. This creates a blurring effect, leading to decreased resolution.

5. Discussion and future work

This work provides additional insight into the first-ever measurements using a dysprosium converter with a scintillator material to produce indirect digital neutron radiographs. While the scintillator material itself is gamma-sensitive, activating the dysprosium converter in the beamline to produce an image and then physically transferring it to a digital imaging system produces a gamma-insensitive process. This is significant because it allows neutron radiography of radioactive samples without gamma-ray interference. Utilizing this technique to take advantage of the quicker acquisition times of digital neutron radiography allows for the possibility of conducting digital radiography in a matter of minutes, enabling neutron tomography on radioactive samples in a single day. A conceptual design of how such imaging would occur is shown in Fig. 11.

The successful demonstration of gamma-discriminating digital transfer method neutron imaging is the first step towards developing a system capable of neutron radiography on irradiated nuclear fuels. The next step is to improve the performance of the scintillation screens so they can generate improved radiographs. ^{164}Dy comprises only 28.18% of natural dysprosium. Therefore, using scintillation screens consisting of enriched ^{164}Dy could improve detector efficiency by

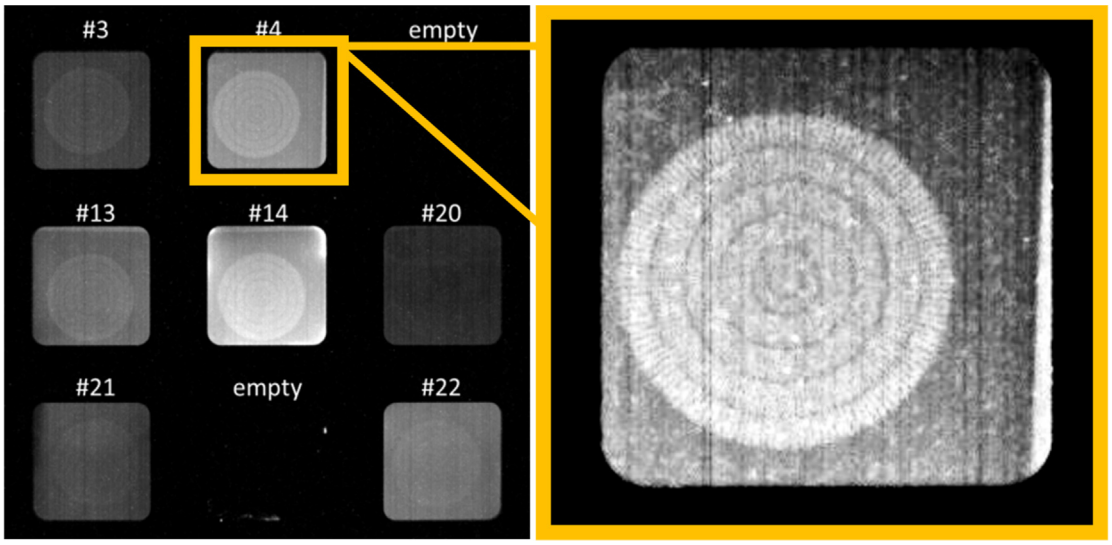

Fig. 10. (Left) Neutron radiograph of a Siemens star for each scintillator. (Right) A magnified neutron radiograph of the Siemens star acquired using screen #4.

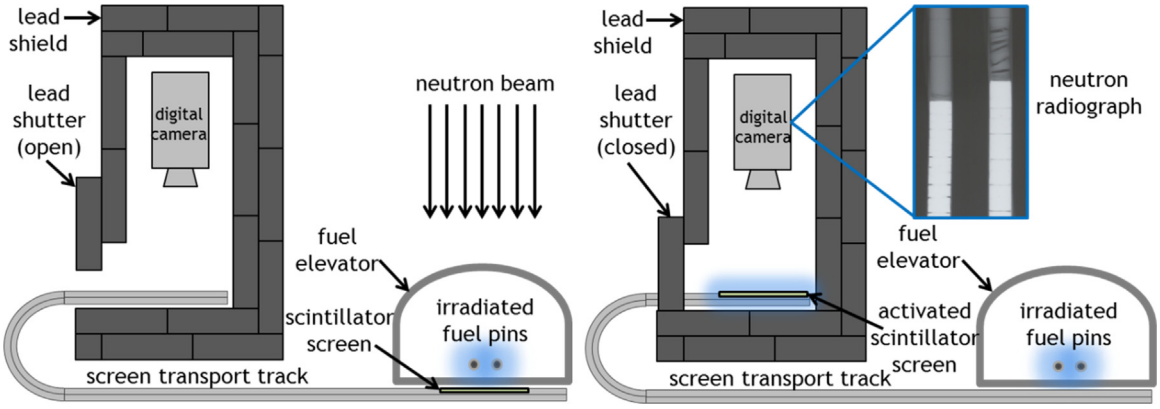

Fig. 11. Illustration of the digital indirect neutron imaging with scintillator screen concept. (Left) The screen is placed in the beamline and exposed behind the imaging object. (Right) The screen is then transported away from the fuel into the camera box and the digital camera captures the latent image on the scintillator screen. [7].

almost threefold. Additional converter materials such as ^{115}In could also be examined to determine if they provide improved performance.

A potential future application of this work is to perform neutron computed tomography on irradiated nuclear fuel using the digital neutron transfer method. Further screen testing is needed to optimize neutron detection before neutron radiography of irradiated materials is performed, along with efforts to perform neutron tomography. Advanced image processing will be required to perform neutron tomography with these screens because images will retain a history of previous acquisitions from the longer-lived isotope with the 2.33-hour half-life. It may also be necessary to employ multiple dysprosium-based screens so that the camera can read one screen while another is in the beamline, which would reduce total acquisition time for neutron tomography and reduce the impact of image history build-up.

CRediT authorship contribution statement

Aaron E. Craft: Conceptualization, Developed the methodology for measurements, Provided resource for performing these measurements, Funding acquisition, Project administration, Writing - review & editing. **William C. Chuirazzi:** Performed the formal analysis of the data, Writing - original draft, Writing - review & editing. **Christian Grünzweig:** Conceptualization, Project administration for activities at PSI. **Manuel Morgano:** Developed the methodology for taking the measurements, Performed the measurements investigating the screen performance, Performed the initial formal analysis of the data, Writing the report that fed into the manuscript. **Eberhard H. Lehmann:** Conceptualization, Project administration for activities at PSI.

Declaration of competing interest

The authors declare that they have no known competing financial interests or personal relationships that could have appeared to influence the work reported in this paper.

Acknowledgments

This work is based on experiments performed at the Swiss spallation neutron source SINQ, Paul Scherrer Institute, Villigen, Switzerland. Work funded through the INL Laboratory Directed Research & Development (LDRD) Program under DOE Idaho Operations Office Contract DE-AC07-05ID14517. LDRD Project ID# 17A1-093FP.

References

[1] A.E. Craft, J.D. Barton, Applications of neutron radiography for the nuclear power industry, Physics Procedia 88 (2017) 73–80.
[2] A.E. Craft, D.M. Wachs, M.A. Okuniewski, D.L. Chichester, W.J. Williams, G.C. Papaioannou, A.T. Smolinski, Neutron radiography of irradiated nuclear fuel at Idaho National Laboratory, Physics Procedia 69 (2015) 483–490.

[3] A.E. Craft, G.C. Papaioannou, D.L. Chichester, W.J. Williams, Conversion from film to image plates for transfer method neutron radiography of nuclear fuel, Physics Procedia 88 (2017) 81–88.
[4] G.C. Papaioannou, A.E. Craft, M.A. Ruddell, Conversion from film based transfer method neutron radiography to computed radiography for post irradiation examination of nuclear fuels, Mater. Res. Proc. 15 (2020) 136–141.
[5] S.R. Jensen, A.E. Craft, G.C. Papaioannou, W.W. Empie, B.R. Ward, L.A. Batt, Restart of the transient reactor test (TREAT) facility neutron radiography program, Nucl. Technol. 205 (2019) 1325–1335.
[6] P. Vontobel, M. Tamaki, N. Mori, T. Ashida, L. Zanini, E.H. Lehmann, M. Jaggi, Post-irradiation analysis of SINQ target rods by thermal neutron radiography, J. Nucl. Mater. 356 (2006) 162–167.
[7] A. Craft, C. Grünzweig, M. Morgano, W. Chuirazzi, E. Lehmann, Gamma discriminating scintillation screens for digital transfer method neutron imaging, Mater. Res. Proc. 15 (2020) 74–79.
[8] E.M. Baum, H.D. Knox, T.R. Miller, Chart of the Nuclides, 16th ed., Knolls Atomic Power Laboratory, 2002.
[9] E.H. Lehmann, P. Vontobel, L. Wiezel, Properties of the radiography facility NEUTRA at SINQ and its potential for use as european reference facility, Nondestruct. Test. & Eval. 16 (2001) 191–202.
[10] E. Lehmann, P. Trtik, D. Ridikas, Status and perspectives of neutron imaging facilities, Physics Procedia 88 (2017) 140–147.